

SMALL-SIZE SPACE DEBRIS DATA COLLECTION WITH EISCAT RADAR FACILITIES

J Markkanen, M Postila and A van Eyken

Executive Summary
of
ESOC Contract No. 18575/04/D/HK(SC)
with
EISCAT Scientific Association

ESA/ESOC Technical Management
H Klinkrad and M Landgraf



June 2006
July 2006 (revised)

EUROPEAN SPACE AGENCY
CONTRACT REPORT

The work described in this report was done under ESA contract.
Responsibility for the contents resides in the authors or organizations that prepared it.

Generated from L^AT_EX source, July 27, 2006.

ESA study contract summary page

<p>ESA CONTRACT No 18575/04/D/HK(SC)</p>	<p>SUBJECT: Small-size Space Debris Data Collection with EISCAT Radar Facilities</p>	<p>CONTRACTOR: EISCAT</p>
<p>ABSTRACT</p> <p>The present study is the third in a series of our ESA contracts since 2000 to develop, implement, and apply a method of using the EISCAT ionospheric research radars, located in northern Norway near Tromsø (site latitude 69.5°, radar wavelength 32 cm) and in Longyearbyen on Svalbard (78.1°, 60 cm), to measure space debris simultaneously with the standard ionospheric measurements. In the present contract, the emphasis has been in performing a significant number of debris measurements. We have accumulated about 10 000 debris events during more than 800 hours of measurements in 2004 and 2005.</p> <p>A basic aim through this series of studies has been to be able to conduct the debris measurements in a “piggy-backed” mode, without interfering with the standard EISCAT measurements. We utilize the radar's analog signal and the frequency reference, but otherwise place no requirements whatsoever on the host's resources or operations. Especially, we take both the radar transmission schemes and the antenna pointing directions as given, and optimize their use for our purposes. We use a special digital receiver back-end, connected in parallel with the standard EISCAT receiver at some point in the analog signal path. For increased detection sensitivity, we implement coherent pulse-to-pulse integration by computing the radar ambiguity function from a segment of measured transmission and reception that typically covers coherently a few tens of interpulse periods, 0.2-0.3 seconds. At the Tromsø radar, 0.2 s coherent integration gives 50% probability of detection of a 2.1 cm sphere at 1000 km range. At the Svalbard radar, the corresponding minimum detectable diameter is 2.9 cm. At the Tromsø system, typical integrated detection rate over LEO is 15-20 events per hour, on Svalbard, about twice as much.</p> <p>Even though we have been able to obtain good sensitivity and reasonable event rates, there are inevitably limitations with our approach. Partly these are due to using radars that have been designed for beam-filling soft targets rather than small hard targets, partly due to the inherent difficulty of coherent integration, and partly due to the piggy-backed nature of our measurements. First, even though it seems that the coherent integration increases detection sensitivity somewhat, it is very difficult to get quantitative control on the integration loss, especially in the common EISCAT case of multi-frequency transmission. Second, none of the EISCAT antennas is equipped with a monopulse feed, so the target's path across the radar beam is not known, and only a lower bound for the radar cross section can be estimated. An unknown proportion of the events represents side-lobe detections. Third, the dominant pointing directions in EISCAT are towards south at about 70-80 degrees elevation, which makes it difficult to estimate Doppler-inclination.</p> <p>In spite of the limitations, EISCAT space debris measurements, summarized in this report and available in detail on the CD accompanying the Final Report, taken with two wavelengths, at two high latitude locations, in long continuous measurements (weeks), sometimes with multiple pointing directions, present an interesting check of the debris models in LEO. Some further work, however, remains to be done before quantitative comparison to the models, such as ESA's MASTER model, can be made with confidence. For instance, it seems desirable to re-detect the debris events with non-coherent pulse-to-pulse integration, a process which would be entirely possible since we routinely save the raw data of all the events.</p>		
<p>The study was carried out by the following team members: J. Markkanen, M. Postila (Study Manager) / EISCAT</p>		
<p>ESA Study Manager: Heiner Klinkgrad, Markus Landgraf, ESOC</p>		

Contents

1 Overview	5
1.1 Introduction	5
1.2 Study objectives	7
1.3 Work done	7
1.4 For future work	8
2 Theory	9
2.1 The match function method	9
2.2 Non-coherent integration in the match function method	12
2.3 Comparison of coherent and non-coherent integration	13
3 Measuring system	14
3.1 Hardware	14
3.2 Software	18
4 Measurements	20
4.1 MANDA campaigns in August 2005 and November 2005	20
4.2 CP2 campaign in September 2005 at Tromsø UHF radar	24
4.3 Test measurement at ESR in November 2005	27

1 Overview

1.1 Introduction

It is estimated that there are more than 200 000 objects larger than 1 cm currently orbiting the Earth as an enduring heritage of four decades of space activity. This includes the functioning satellites, but by far the bulk of the objects represent what is called space debris (SD), man-made orbital objects which no longer serve any useful purpose. Many of the small-sized (less than 10 cm) particles are due to explosions of spacecraft and rocket upper stages, but there are also exhaust particles from solid rocket motors, leaked cooling agents, and particles put into space intentionally for research purposes. The large (> 10 cm) objects have known orbits and are routinely monitored by the US Space Surveillance Network, but information of the smaller particles is fragmentary and mainly statistical. In particular, no radar in Europe is routinely used for monitoring small-sized SD.

This report describes the third study in a series of of ESA contract work that started in 2000–2001 with a study about the feasibility of using the EISCAT ionospheric research radars for space debris measurements (3). Since the early 1980's, the EISCAT mainland radars—the Tromsø UHF radar operating at 930 MHz and the VHF radar operating at 225 MHz—have been performing ionospheric measurements on the order of 2000 hours per year; and since the late 1990's, after the EISCAT Svalbard radar (ESR) became operational, EISCAT has been measuring more than 3000 hours annually. The goal is to use a substantial proportion of these operating hours for simultaneous space debris measurement in cost-effective way. In the first study, it was shown that it is feasible,

1 Overview

and technically straightforward, to perform SD measurements in parallel with normal EISCAT ionospheric measurements, without interfering with those measurements (6).

Our measuring approach, introduced in the initial study, is to operate a separate digital receiver back-end, which we call the SD receiver, in parallel with the EISCAT standard digital receiver. This allows us to implement pulse-to-pulse coherent integration via a method which we call the match function (MF) method. Essentially our MF is what is often called the radar ambiguity function in the literature. The coherent integration is achieved by computing the MF as function of range and velocity for a set of values, and finding the maximum of the function. For a coherent signal, the maximum value of the MF gives an estimate of the total signal energy. Target detection is based on the maximum value exceeding a predefined threshold. The position of the maximum gives estimates of target range and radial velocity.

To make the hardware as simple and cheap as possible, the custom-made part of the SD receiver is basically just a fast sampler and digital demodulator; the MF computations are done in fast but still cheap general purpose workstations. The SD receiver samples the EISCAT analog signal, at the second intermediate frequency (around 10 MHz) level, fast enough to capture the relevant frequency channels into a single digital stream, without doing the customary channel separation. Typically during a measurement, we sample at the rate of about a million complex samples per second continuously, producing more than 10 GBytes of data per hour.

A straightforward implementation of the MF method implies long data vectors, with lengths of hundreds of thousands complex points, to be Fourier-transformed a few thousand times per every second of raw data; basically, one is computing power spectra for a relatively large number of range gates. At the Third European Conference on Space Debris in 2001, we had to concede that with the processing speed that we had achieved at the time, it would take several centuries of CPU time to analyze just one year's quota of EISCAT space debris measurements. However, soon afterwards, M Lehtinen of Sodankylä Geophysical Observatory, who was the project leader of the first study, realized that by accepting some loss of detection sensitivity and a small bias in the velocity estimate, it would be possible to speed up MF computation drastically, typically by more than two orders of magnitude. We use the term fast match function algorithm (FMF) for the resulting computation scheme. The FMF algorithm is central to our practical work. It is described in (8), and also sketched in Fig. 1.

Our second study (4) was conducted in 2003–2004. The main purpose was to develop the measuring and analyzing system to be capable of handling large amount of measurements, hundreds of hours per year. The key task was to boost the system performance so that target detection and parameter estimation could be done in real-time, to avoid excessive piling-up of data, and also to make a more or less interactive inspection of the data feasible. In the final report of the second study (7), we gave a detailed analysis of several aspects of the MF-method, both in its the basic form, and when using the fast variant. We described the measuring and analysis software in considerable detail. We were also able to show the results of about 150 hours of debris measurements, all conducted at the Tromsø 930 MHz radar. Our first longer, 100 hour, campaign was run in November 2004. Before the 100 hour run, we took part in the international beam park 2004 debris campaign by collecting 17 hours of data in September 2004

After our first two ESA contracts had established the feasibility of using EISCAT radars for SD measurements, and had built sufficient machinery to handle the data in practice, the present contract was signed late in 2004, for the purpose of finalizing the

data processing and applying it to produce a fairly large amount of debris measurements (5).

1.2 Study objectives

According to our contract, the overall objective of this study was to prepare for an operational phase of routine space debris measurements during the standard EISCAT ionospheric measurements, based on the developments in the two precursor studies.

The contract work was divided to five work packages, which were grouped into two phases. Phase one was to cover the first two work packages during 2005; whether or not to continue the study to phase two, was left to be decided later on. Either party had the option to discontinue the contract after phase one. In project meeting on February 14th 2006 at ESOC, it was unanimously agreed that, due to shortage of resources, the phase two would not be activated. This report therefore covers only the phase one of the study, the work packages W.P. 1: Updating of the data processing methods and algorithms, and W.P. 2: Routine space debris measurements during common programme measurements.

1.3 Work done

W.P.1 Updating of the data processing methods and algorithms

Under this work package, the following development has taken place.

- ▷ Grouping detector hits to events has been much enhanced by improving the preprocessor of the event-grouping program DARC, the bad-hit removing Matlab program CLEANSCANS. The updated CLEANSCANS can work automatically, and is nearly as effective in performing the required tasks as an interactive operator.
- ▷ Throughout these studies, a persistent puzzle has been the loss of coherence in the coherent integration, and the resulting effect on detection sensitivity and RCS estimation. In the final report of the second study (7) we have already inspected the effect of multiple frequencies, the effect of target acceleration, and the consequences of using FMF instead of MF, and we will not repeat the work here. In the present work we have attempted to understand better the issue of coherent versus non-coherent integration. We started experimenting with non-coherent pulse-to-pulse integration for the first time when analyzing the data from EISCAT's participation in the 2004 beam park experiment, and found that there was little difference in the number of events that came through from the final analysis. We describe our implementation of non-coherent integration in section 2.2; this has not been done in the earlier reports. In the Final Report of the present study (9) we derive the expected difference between coherent and non-coherent integration; but here we skip the derivation, and only show a set of curves of detection sensitivity for the two integration modes in Fig. 2. Even with fully efficient coherent integration, the expected gain in terms of the weakest detectable signal is rather small, about 5–6 dB with 0.3 s integration time. With real data it is then entirely possible to lose most if not all of the advantage to the mentioned sinks of coherence, especially, when one has to handle a multi-frequency experiment. Nevertheless, in our implementations, the FMF-based coherent integration executes faster than a corresponding non-coherent integration, and tends to be slightly more sensitive,

so we are going to use FMF for the initial detection also in the future. The ideal solution might be some kind of hybrid integration scheme.

W.P.2 Routine space debris measurements during common programme measurements

For this work package, we have done the following.

- ▶ The SD receiver is installed in Tromsø, and only requires powering-up to be ready to start data collection. Powering-up requires somebody to push a button in Tromsø; the measurements themselves can be controlled over the internet from any EISCAT site. The hardware has worked reliably at Tromsø.
- ▶ Most of the user interface for space debris measurement, which we call DROS, was built during the previous contract. The DROS system has been used routinely, in all the measurements made for this contract, to take care of the data recording. The DROS is basically an enhanced copy of the EROS system which controls all the EISCAT radars.
- ▶ During 2005, we measured SD for about 700 hours, collecting about 8000 events. All the measurements were made in parallel with EISCAT CP measurements. The measurements were concentrated in four campaigns described in chapter 4, where we show a few summary figures; several more figures are shown in the Final Report. Lists of event parameters and summary plots for all events are on the CD accompanying the Final Report.
- ▶ We ran a 24 hour test measurement at the ESR site on November 10th, 2005. The measurement is described in section 4.3, and the measurement results are included on the CD. It is quite clear that the ESR system is well suited for these measurements.

1.4 For future work

The preparatory work needed to apply the ESA PROOF tool to EISCAT data was not covered by the two work packages under the present contract. Further work is needed before the collected data can be used quantitatively to test the debris models. A task would be to make sure that the PROOF tool can handle arbitrary antenna beam shapes, side-lobes included, so that no particular distinction needs to be done concerning side-lobe detections. The other task would be to resort to non-coherent pulse-to-pulse integration in target detection, because it is very difficult to get quantitative control on the integration loss in the coherent integration. It appears that our coherent integration is *somewhat* more sensitive than the customary non-coherent integration, but to quantify the difference reliably in practice seems difficult. We therefore suggest to re-detect the collected data using non-coherent integration with sufficiently high detection threshold. This would result in some loss in the number of finally available events, but would give a firmer handle on the statistical properties of the events. A re-detection test with one of the four data sets taken during this contract found 667 events with non-coherent integration, out of the 801 events originally detected with FMF-based coherent integration. We have saved the raw data (about 400 GBytes) of all our events permanently to hard

disk, so this approach is entirely feasible.

2 Theory

2.1 The match function method

The complex-valued signal $z(t)$ consists of target echo $s(t)$ and noise,

$$z(t) = s(t) + \gamma(t). \quad (1)$$

During a time interval $[0, T_c]$, the integration time—we typically use $T_c = 0.2\text{--}0.3$ s— $s(t)$ is modeled as a delayed-in-time, Doppler-shifted replica of the transmission $x(t)$,

$$s(t) = b_0 x(t - 2R_0/c) e^{-i2\pi \frac{v_0}{\lambda/2} t}, \quad (2)$$

where R_0 is target range, v_0 is target radial velocity in the radar frame of reference, and λ is the radar wavelength. In EISCAT space debris measurements, in addition to $z(t)$, also $x(t)$ is measured, so that Eq. (2) provides a three-parameter set of model functions to be matched against the measured $z(t)$.

We assume that the echo stays coherent, that is, the model Eq. (2) holds, during the integration time, a few tens of interpulse periods (IPPs). Then it is possible to use coherent integration in target detection. The match function method of coherent pulse-to-pulse integration is based on computing the quantity that is often called the radar ambiguity function in the literature, but which we choose to term the match function, MF. References (6) and (8) present the match function method from the point of view of Bayesian statistical inversion. Here we give a less rigorous description, which also omits complications that arise when we apply the method in practice in EISCAT, such as the need to correct for target acceleration and to handle multiple frequency channels. The match function is a function of the range gate $R_j = j\tau_s c/2$, where τ_s is the sampling interval, and the Doppler-velocity v , which is the radial component of the velocity vector (positive away from the radar). The MF is computed from the sampled signal vector \mathbf{z} and the transmission-sample vector \mathbf{x} as

$$\text{MF}(v, R_j) = \frac{|\sum_n z_n \bar{x}_{n-j} e^{i2\pi \frac{v}{\lambda/2} n\tau_s}|}{\|\mathbf{x}\|}, \quad (3)$$

where

$$\|\mathbf{x}\| = \left(\sum_n |x_n|^2\right)^{1/2}. \quad (4)$$

It follows from Eq. (3) that at the velocity points

$$v_k = \frac{k}{N_{\text{DFT}}} \frac{\lambda}{2} \frac{1}{\tau_s} \quad (5)$$

the MF can be computed using discrete Fourier-transform. For a fixed range, the function $v \mapsto \text{MF}(v, R_j)$ is essentially the spectrum of the cross-correlation vector $\mathbf{w}^{(j)}$: $w_n = z_n \bar{x}_{n-j}$; we refer to it as the MF velocity slice through the range R_j . Figure 1 summarizes the match function computation. There we also show an extra step that we normally

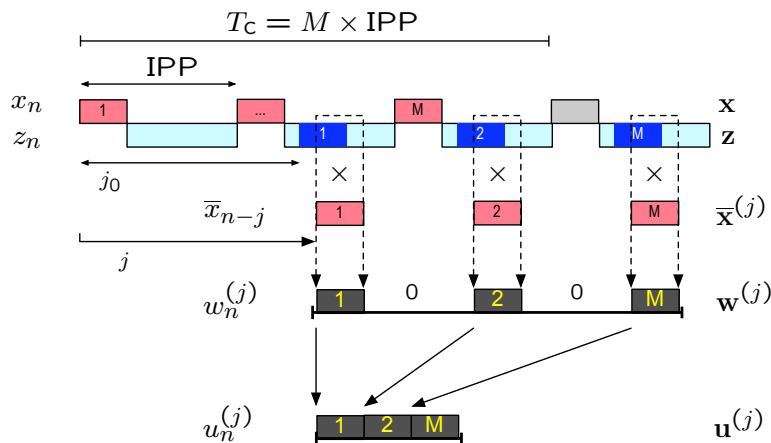


Figure 1: Coherent integration of M pulses in the MF- and FMF-algorithms. The raw data are the complex transmission samples x_n and the noisy reception samples $z_n = s_n + \gamma_n$. The diagram also indicates an echo of a point-target at range R_{j_0} . To evaluate the match function $\text{MF}(R, v)$ at range R_j and velocity v_k , the first step is to point-wise multiply the reception vector \mathbf{z} with the time-shifted, complex-conjugated transmission vector $\bar{\mathbf{x}}^{(j)}$, to produce the vector $\mathbf{w}^{(j)}$. The magnitude of the discrete Fourier-transform of $\mathbf{w}^{(j)}$, normalized by $\|\mathbf{x}\|$, gives a velocity slice of the match function: $\text{MF}(j, k) = |\text{DFT}\{\mathbf{w}^{(j)}\}(k)|/\|\mathbf{x}\|$. Computation of the fast match function FMF has an extra step before the Fourier-transform: the M non-zero blocks of $\mathbf{w}^{(j)}$ are concatenated, to the much shorter vector $\mathbf{u}^{(j)}$. The normalized magnitude of $\text{DFT}\{\mathbf{u}^{(j)}\}$ is a velocity slice in the FMF.

take to speed up the computations: basically, we just drop out the “unnecessary” zeros that occur in the DFT input vector due to the pulsed transmission. We call the resulting algorithm the fast match function algorithm, FMF. The gain of speed is large, typically more than two orders of magnitude, so we almost always use FMF in the practical computations. The gain in speed comes with a price, since the detection sensitivity in the FMF-scheme is slightly reduced compared to the MF.

If there is no noise, the position of the MF maximum gives the target range R_0 and radial velocity v_0 ,

$$\arg \max_{v, R} \text{MF}(v, R) = (v_0, R_0),$$

and the value of the maximum is proportional to the square root of the total signal energy E_s ($\propto \|\mathbf{s}\|^2$). Even with noise, we use the position of the MF maximum as an estimate of the target range and Doppler-velocity,

$$(\hat{v}, \hat{R}) = \arg \max_{v, R} \text{MF}(v, R), \quad (6)$$

and expect the MF maximum value still to be a reasonable estimate for $\|\mathbf{s}\|$. With noise, we need also consider background subtraction. We assume that the maximum of the noisy MF takes place near the position (v_0, R_0) , and form the expectation value of MF^2 . Assuming that the noise samples γ_n are zero mean, independent, complex gaussians with

variance σ^2 , one gets

$$\mathbb{E}(\max \text{MF}^2) \approx \|s\|^2 + \sigma^2. \quad (7)$$

This shows that to get an unbiased estimate of $\|s\|^2$, we have to subtract the noise power from the MF^2 maximum value,

$$\widehat{\|s\|^2} = \max \text{MF}^2 - \sigma^2. \quad (8)$$

With coherent integration, the minimum detectable signal will have $\max \text{MF}^2 \gtrsim 25 \sigma^2$ in our case, so the subtraction has only a minor effect to the estimate. With non-coherent integration, the background subtraction is essential.

The norm $\|s\|$ of the received signal is related to the actual energy $E_{s'} = \int |s'(t)|^2 dt$ of the incoming signal $s'(t)$ in front of the receiver by

$$\tau_s \|s\|^2 = g E_{s'}, \quad (9)$$

where τ_s is the sampling interval, provided that the signal is of sufficiently narrow bandwidth so that there is not much aliasing, and that the receiver power gain g can be taken to be constant across the signal bandwidth. We divide the receiver gain such that $g = g_A \cdot G$, where g_A is the gain of the relatively wide-band analog receiver and G is the precisely calculable gain of the digitally implemented space debris receiver. We take g_A to be a constant over the whole bandwidth of the SD receiver. We get rid of the unknown gain g_A by noting that the noise power after the receiver, σ^2 , estimated as the variance of the reception samples z_n in the absence of signal, is

$$\sigma^2 = k_B T_{\text{sys}} g_A B_{\text{eq}}, \quad (10)$$

where B_{eq} is the noise-equivalent bandwidth of the SD receiver, and $k_B T_{\text{sys}}$ is the power spectral density of the wide-band noise in front of the receiver, which we take to be a known radar parameter. The impulse response of the SD receiver is constructed to be of constant value $1/\tau_s$ and duration equal to τ_s . For such a system, $B_{\text{eq}} = 1/\tau_s$ so that, from Eq. (8)–(10), we get

$$\frac{\widehat{E}_{s'}}{k_B T_{\text{sys}}} = \frac{1}{G} \left(\frac{\max \text{MF}^2}{\sigma^2} - 1 \right). \quad (11)$$

In practice, we take G to be unity, and drop the prime from $E_{s'}$. We call the dimensionless ratio of the total signal energy divided by the noise power spectral density (= noise power per unit bandwidth) the “energy-to-noise ratio” ENR,

$$\text{ENR} \equiv \frac{E_s}{k_B T_{\text{sys}}}. \quad (12)$$

Thus, we estimate the energy-to-noise ratio from the MF maximum value as

$$\widehat{\text{ENR}} = \frac{\max \text{MF}^2}{\sigma^2} - 1. \quad (13)$$

Equation (13) has two related uses. First, it gives the target detection criterion for the threshold detection: with threshold Θ ,

$$\text{detection} \leftrightarrow \sqrt{\widehat{\text{ENR}} + 1} > \Theta. \quad (14)$$

2 Theory

We try to set the threshold Θ to be so high that there are only “very few” false alarms. Experience has shown that, with the coherent integration times 0.2–0.3 s that we normally use with the EISCAT standard experiments, the value $\Theta = 5$ is a suitable starting point. In the Final Report we give some theoretical justification for that choice, showing that it corresponds to a false alarm time of a few hours. The standard threshold might need to be increased sometimes, typically during strong auroral events, due to clutter. Then we normally increase Θ perhaps up to 7, but only in those ranges where the ionospheric clutter actually is a problem. On the other hand, we try to keep the threshold setting intact during a single measurement campaign. Normally the ionospheric clutter is a problem only at altitudes up to about 500 km, and their range aliases.

The second use of Eq. (11) is to estimate the target “size”. We treat the system temperature as a known radar parameter, and use the measured MF maximum to get estimate of the ENR. We use these to find a lower limit, RCS_{\min} , for the target’s radar cross section (RCS). From the standard radar equation it follows

$$\text{RCS} = \frac{(4\pi)^3 k_B T_{\text{sys}} \cdot R^4 \cdot \text{ENR}}{G(\phi)^2 \cdot \lambda^2 \cdot P_x \cdot \mathcal{D}T_c}. \quad (15)$$

Here R is target range, λ is radar wavelength, P_x transmission peak power, \mathcal{D} transmission duty cycle so that $\mathcal{D}T_c$ is the actual length of transmission during the integration T_c . The factor $G(\phi)$ is the antenna power gain in the direction of the target within the radar beam, an angle ϕ offset from the known direction of the antenna optical axes. In the EISCAT system, it is normally not possible to find the offset angle. As a way of cataloguing the observed signal strength, we therefore normally quote RCS_{\min} , which we get from Eq. (15) by setting $\phi = 0$.

2.2 Non-coherent integration in the match function method

We always process a single pulse coherently. We will use the expression “non-coherent integration of M pulses”, when we compute r.m.s of the single-pulse match functions. Using non-coherent integration places less demands for the coherence time of the signal. On the other hand, if the signal is coherent, phase information is unnecessarily lost in the squaring. More precisely, we implement the non-coherent integration via maximization, over the range and velocity parameters, of the non-coherent match function MF_{nc} , which we define by

$$\text{MF}_{\text{nc}}(R, v) \equiv \sqrt{\frac{1}{M} \sum_{m=0}^{M-1} [\text{MF}(m; R, v)]^2}. \quad (16)$$

This is a smoothed version of any of the M single-pulse MFs. Therefore, the maximum value of $\text{MF}_{\text{nc}}^2/\sigma^2$ is roughly equal to the sum of the background level (unity) and the mean of the energy-to-noise-ratios computed separately for each pulse:

$$\frac{\max_{v,R}(\text{MF}_{\text{nc}})^2}{\sigma^2} \approx 1 + \frac{\text{ENR}}{M}. \quad (17)$$

The detector program DSCAN has been enhanced to handle non-coherent integration in accordance to Eq. (16).

In the Final Report we estimate how much more detection sensitivity we can expect from fully coherent integration compared to the non-coherent integration, in specific

2.3 Comparison of coherent and non-coherent integration

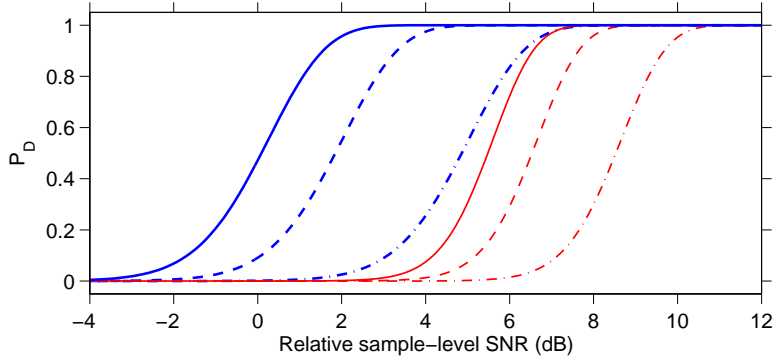


Figure 2: Probability of detection in the Tromsø MANDA experiment. The six curves are, from left to right, for 0.3, 0.2 and 0.1 s coherent integration, and for 0.3, 0.2 and 0.1 s non-coherent integration. The signal-to-noise ratio SNR means the quantity $|s/\gamma|^2$ computed from unprocessed data $z_n = s_n + \gamma_n$. The reference level 0 dB is the level that gives 50% probability of detection with 0.3 s coherent integration. It can be seen that with 0.3 s integration, coherent integration is about 5 dB more sensitive than non-coherent integration on this measure.

experiment schemes. Figure 2 shows the probability of detection as a function of sample-level signal-to-noise ratio $\text{SNR} = |s|^2/|\gamma|^2$, for a few integration times, both in coherent integration and in non-coherent integration. For example, with 0.3 s integration time, coherent integration is expected to allow the detection of about 5 dB weaker signals than non-coherent integration.

2.3 Comparison of coherent and non-coherent integration

Figure 2 suggests that with a 0.3 s coherent integration we should be able to detect about 5.4 dB weaker signals than with 0.3 s non-coherent integration. But several factors tend to reduce the sensitivity in practice. First, the much shorter data vectors to be Fourier-transformed in the non-coherent integration allow heavy zero-padding of the input vector. This in practice eliminates the “picket-fence” effect from the non-coherent integration. For the picket-fence effect, subtract up to about 4 dB from the MF maximum. Second, use of the FMF algorithm, instead of the the much-too-slow, but more sensitive, basic MF algorithm, can cause an additional loss of up to another 4 dB. Third, in long coherent integrations—and our typical 0.3 s is long in this sense—several dB can be lost if the attempt to compensate for target acceleration fails. Fourth, when the transmission has two frequency channels (a typical case in EISCAT), the two Doppler-shifted spectral lines tend to separate in a long coherent integration, and cannot therefore add in amplitude, even though they are still kept together in the non-coherent integration by virtue of the lower spectral resolution. For this effect, subtract up to 3 dB from the coherently integrated amplitude. These well-understood sinks of the integrated amplitude can add up to a 10–12 dB loss in the worst case. It would not be unexpected to lose about half of that on average, that is, effectively all the 5–6 dB theoretical gain provided by this method. When testing target detection on real data sets with both integration schemes, our experience so far has been that both methods detect nearly the same number of targets.

On the other hand, even though coherent integration perhaps cannot be made signif-

icantly more sensitive in practice than non-coherent integration in the target detection phase, after the detection, more accurate estimates of target parameters are, in principle, available.

3 Measuring system

3.1 Hardware

The EISCAT UHF radar

In most of our SD measurements so far, we have used the EISCAT UHF radar (1; 2). The 32 m UHF antenna is a fully steerable parabolic dish, with Cassegrain optics, and features a maximum rotation rate of about $80^\circ/\text{min}$ both in azimuth and elevation. The antenna pointing direction is calibrated using celestial radio sources, and is believed to be accurate better than 0.1° in most directions.

A block diagram of the UHF radar at the Tromsø site is shown in Fig. 3. The Tromsø UHF receiver has a cooled preamplifier, giving a system temperature $T_{\text{sys}} \approx 110$ K, much of which is contributed by the transmission/reception switch necessary to protect the receiver during the transmission phase. The radar's radio-frequency (RF) band is centered at 928 MHz, and there are 14 transmission frequencies available, 300 kHz apart. In the most common EISCAT experiment modes, two frequency channels are used. Recently those have been centered at 929.9 MHz (EISCAT frequency F13) and 930.2 MHz (F14). The RF signal is mixed in two stages to the second intermediate frequency (IF2) band, using local oscillators at 812.0 MHz and 128 MHz, so that F13 maps to 10.1 MHz and F14 to 9.8 MHz. The band is formed by the radar's antialiasing filter, which is 6.8 MHz wide and centered at 11.25 MHz.

The EISCAT UHF transmitter consists of a programmable radar controller that generates the pulse patterns at DC level, either uncoded on/off pulses or various classes of binary phase codes; an exciter system that converts the radar controller output to RF around 928 MHz; and a klystron power amplifier that consists of two klystron tubes, in principle capable of delivering a combined peak power of about 2.5 MW. The power during the space debris measurements has been between 1 and 2 MW. The maximum transmitter duty cycle is 12.5%, and duty cycles near this value are also used in most experiments in practice. The time and frequency base at all EISCAT sites is taken from the GPS system.

The EISCAT Svalbard radar

Since 1996, EISCAT has operated a 500 MHz radar system in Longyerbyen, Svalbard (10). The system has two antennas: a steerable 32 m dish and a fixed 42 m dish, pointed to the magnetic-field aligned direction. The radar has a single transmission system, capable of a peak power of about 1 MW, with the high duty cycle of 25%. The transmission power can be switched to either of the two antennas on pulse-to-pulse basis, by reversing the phase of the RF drive to one half of the 8-module transmitter power amplifier. The normal mode of operation, however, is to alternate between the antennas much less frequently, typically once every few seconds. A special problem at the ESR is ground clutter, for the radar has an unhindered field of view over a fjord to

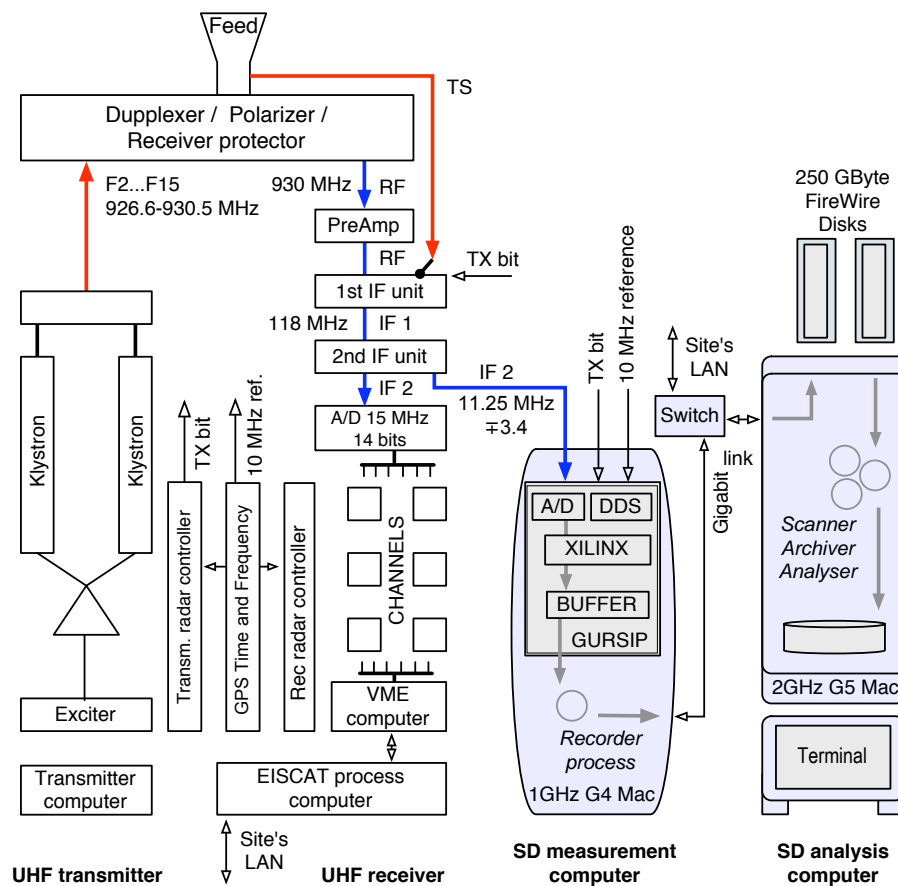


Figure 3: The space debris receiver connected to the EISCAT UHF radar. The SD receiver consists of a measurement computer and an analysis computer. The measurement computer hosts a custom signal processing board (GURSIP). The primary analog input to the SD receiver is the EISCAT second intermediate frequency (IF 2) band. The input contains, time-multiplexed, both the standard received signal and the transmission sample signal (TS). On the processing board, there is an analog-to-digital converter (A/D) taking 40–46 megasamples per second; a direct-digital-synthesizer chip (DDS), which provides clock signals on the board, phase-locked to the host radar’s 10 MHz frequency reference signal; two Xilinks signal processing chips (XILINX) to perform signal demodulation and sampling rate reduction; and a memory buffer for temporary storage of the samples. The recorder program running on the measurement computer moves the samples over a gigabit network link to external FireWire disks, mounted on the analysis computer. Target detection is done by the scanner program running on the analysis computer, using the FMF-method. After detection, two other software modules, the archiver and the analyser, store away the event’s raw data, and estimate and save the target parameters.

3 Measuring system

a mountainous landscape reaching to the distance of more than 70 km. Figure 4 shows a block diagram of the ESR system and the connection of the SD receiver.

The space debris receiver

Figure 3 shows the main blocks of the SD receiver, connected to the EISCAT UHF system at the Tromsø site. The arrangement at the ESR site is quite similar and is illustrated in Fig. 4.

The EISCAT standard data processing handles a multi-frequency transmission by feeding the IF2 data to multiple hardware channels, each tuned to a particular center frequency. In the SD receiver, we sample the analog IF2 band fast enough to capture the relevant frequency channels into a single digital stream.

In addition to the standard reception, our data processing requires that the transmission waveform is measured. EISCAT provides the transmission sample signal (TS) time-multiplexed into the same data path as the reception. The multiplexer switch is controlled by the receiver protector bit (“TX bit”), generated by the EISCAT radar controller microprocessor. We routinely record the receiver protector bit into our data stream to mark out the transmission blocks.

The core of the data acquisition system is a custom PCI-board which performs sampling, quadrature detection and sampling rate reduction. The board was developed originally for ionospheric tomography by the now defunct Finnish company Invers Ltd.

The sampling rate f_A of the A/D converter on the PCI board can be programmed (at least) between 40 and 46 MHz. The resulting real-valued sample stream is processed by programmable logic chips, from the Xilinx SpartanXL family, to perform quadrature detection, essentially by doing Hilbert transforms. The result of the transform is a complex-valued sample stream at the sampling frequency $f_A/4$, representing the negative frequency part of the spectral contents of the analog input. The chip then decimates the 10–11.5 MHz stream to the final sampling rate. A typical decimation factor M_D is 20. The decimation is done by adding samples in blocks of M_D ; this ensures proper filtering. Because frequency translation from IF2 to baseband is done by undersampling, selection of f_A requires careful consideration, to get the frequency channels to map as near to the zero frequency as possible to minimize attenuation in the decimation filter, while at the same time producing a sensible sampling interval as required by our sample-count-based data addressing. In different experiments, we have used 40, 42, 44 and 46 MHz primary sampling rates. Any future version of the SD receiver should have a complex mixer built-in.

The PCI board is mounted in a Macintosh G4 workstation, running under the Mac OS X version of UNIX. We call the Mac G4 the measurement computer. In addition, there is a dual-CPU Mac G5 computer for data analysis. The Mac workstations are connected to each other via a gigabit Ethernet link, and are also connected to the site LAN. The measurement computer runs software from Invers Ltd to read the sample data from an onboard buffer and write them to a hard disk. The data accumulation rate to the disk is between 7 and 30 GBytes per hour, depending on the sampling rate. The LAN connection is used to access the EISCAT process computer, to update the time base in the G4 and G5 once every 5 minutes, using the standard network time protocol. This ensures that the time base in the Macs stays within 20 ms of the time kept in the EISCAT system. This is more than adequate for time-stamping space debris events.

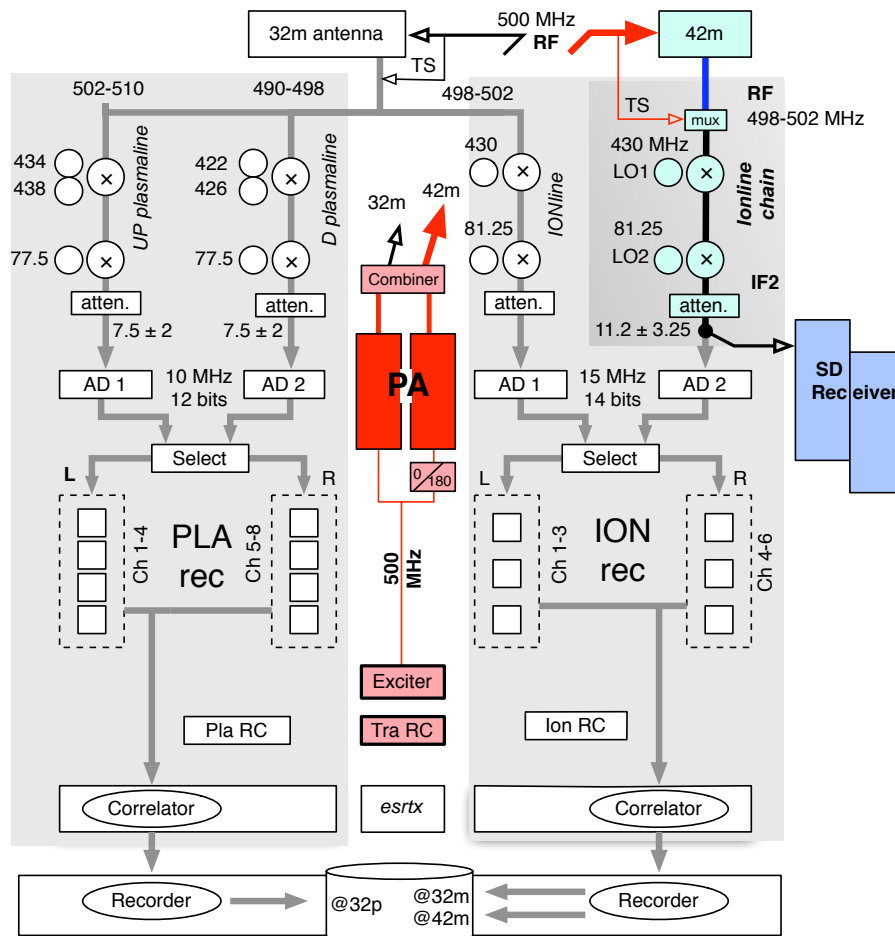


Figure 4: EISCAT Svalbard radar block diagram, showing the principal data flow during the TAU0 CP3 measurement, from the space debris receiver point of view. The radar has a single transmitter, two antennas, and four complete receiver chains. In the TAU0 CP3 scheme, the transmitter output is switched between the antennas every 64 second. While the transmitter is serving the non-steerable 42 m antenna, EISCAT records data only with the ION receiver, and the 32 m antenna is being turned to another direction. The space debris receiver, connected to the second analog IF (IF2) of the receiver chain coming down from the 42 m antenna, records continuously, receiving either the standard echo, or the transmission sample signal (TS). After the 64 second period dedicated to the 42 m system has elapsed, transmission is switched in a few microseconds to the 32 m antenna, by flipping the phase of the exciter output to one half of the transmitter power amplifier, and EISCAT starts recording and transmitting with the 32m antenna. Even though EISCAT is not explicitly making any use of the 42 m system during that time, the ION receiver front-end is kept active, that is, switching between TS-mode and the normal receiving mode. In addition to the analog IF2, the SD-receiver records the control bit (not shown) that switches the system between transmit and receive states. The SD-receiver is phase-locked to the host radar's GPS-derived frequency reference signal.

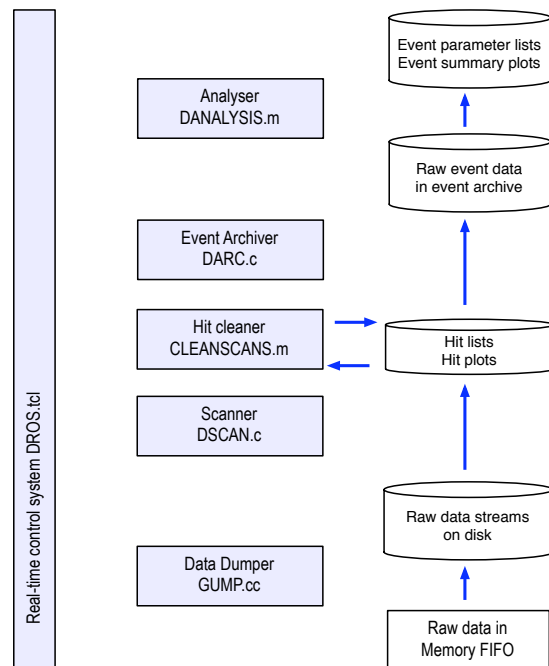


Figure 5: Main modules of the real-time SD data processing software.

3.2 Software

An overview of the real-time SD data processing software system is shown in Fig. 5. The system consists of five main processing units and an overall control system. These have been described in some detail in (7), pp. 57–83. Here we give an updated summary. The processing has the following phases.

Sampling and demodulation. The SD receiver’s programmable firmware delivers complex-valued samples at a strictly regular rate to a buffer, which is visible in the measurement computer’s memory space.

Recording. The recorder program GUMP reads the data from the buffer and writes them to disk files. The sample data are organized into directories which we call the stream directories, or just the streams. Typically, a stream contains 60 minutes of uninterrupted sample flow in time-stamped files, each storing one million complex points as $2 + 2$ byte integers.

Scanning. The streams are processed, one stream at a time, by the SD scanner program DSCAN. Two scanners can be running in parallel in the dual-processor analysis computer. The scanner reads a segment of raw data from a stream and searches through the segment for hard targets range gate by range gate, performing threshold detection using the FMF algorithm. When a pre-determined threshold is exceeded, we say that we have a hit. The scanner saves the hit’s description to a file and proceeds to the next data segment. Scanning is the most time-consuming step in the data processing. DSCAN is implemented as a C program that makes use of the onboard AltiVec vector processor in the G5, by calling routines in Apple’s DSP library. The scanner performance depends strongly on the length of the input data

vector. For the most common configuration ($2 \mu\text{s}$ sampling interval and 0.3 s coherent integration), we get about 2 GFlops mean speed per processor. The output of the scanner is a stream-specific directory in a standard place in the filesystem hierarchy. The directory contains a list of the streams's hits, and for each hit, two Matlab-format files that contain information about the $\text{MF}(R, v)$ associated with the hit. These two files are used by the hit-list cleaning program CLEANSCANS to plot an overview of the match function.

Hitlist cleaning. A problem point in our data processing has long been the interface between detection and analysis, the step that involves grouping the detector hits into events. An event consists of those hits that are caused by a single target when it moves across the radar beam. The hit grouping is handled by the event-archiver program DARC, using only a hit list as its input. If DARC manages to produce a “good” event, the analysis program can in most cases make reasonable sense of it automatically. A hit description in the hit list contains only the most basic parameters, namely, the hit time and the value and location of the MF maximum. We have found that we can much improve the event selection by also taking into account the MF's behavior around the maximum point.

We use the Matlab program CLEANSCANS to remove bad hits from the hit-list file produced by DSCAN. The most common causes of bad hits are range aliased targets and targets which attain their maximum signal strength when the receiver is muted due to ongoing transmission. The problem is that in both case DSCAN triggers on a point which actually is not the true, global, MF maximum, and this leads to seriously wrong estimates of the target range and velocity which are needed in the event forming. While an experienced human operator can normally easily recognize the false maxima based on the look of the MF, finding a suitable computer algorithm was non-trivial. The problem started to unravel only when M Markkanen from the Finnish Eigenor company suggested that we should start making better use of a special property of the MF in EISCAT. With the phase codes that EISCAT customarily uses, the maximum of the MF range profile is a very narrow and high spike, so that a valid maximum not only exceeds the detection threshold, but, crucially, exceeds it much more than its immediate surroundings. By making use of the width of the observed spike, both in the range and the velocity direction on one hand, and by inspecting the level and variance of the local background, CLEANSCANS can now in most cases decide correctly when a hit represents a true MF maximum. Hits which do not represent a true maximum are disregarded.

Event archiving. The next module in the processing chain, the event archiver DARC, inspects the stream's cleaned list of hits, and combines to an event the hits that correspond to a single target passing through the radar beam. Having determined the time boundaries of the event, the archiver copies the event's data to a separate event directory. The event archiver is a C program, but it is not performance critical. Most of its time goes to data copying, so its speed is mainly limited by disk speed. We have archived the raw data for all events from all our measurement campaigns so far, less than 500 GB.

Parameter estimation. As the last step, the analyser program DANALYSER picks events from the event directories and deduces and saves the event parameters. The an-

4 Measurements

alyzer calls DSCAN to re-scan the data using FMF, but with maximum time and range resolution, over a narrow range interval, and to make linear or quadratic fits to the range and Doppler-velocity time series. The range and velocity parameters that we normally quote are taken from these fits, for the time instant of maximum signal strength. The analyser is a Matlab program. The analysis results are written to separate event-specific analysis result directories.

The five main processing blocks run as independent, stand-alone UNIX timesharing processes, which do their specific job once and then die. The processes themselves do not know anything about each other. The processing chain is created and organized by software that we call DROS. The name DROS is a modified version of “eros”, and is meant to indicate that the system is a slightly tailored copy of the standard EISCAT real-time radar operating system. Based on an experiment-specific configuration file and a given start time, the DROS system generates the required input files and command line parameters for the processing modules, starts and restarts the processes in the two computers as required, and maintains and logs state information. The DROS system can query the running EROS at the host radar to find the antenna pointing direction and transmission power information. It is also possible to run each processing component separately via a script; for off-line work, this is the normal mode of operation.

4 Measurements

In accordance to the contract, the 700 hours of measurement, producing about 8000 debris events, were conducted in parallel with standard EISCAT common mode (CP) ionospheric measurement campaigns, using the space debris receiver for data collection.

Manda campaign 11–13 August at EISCAT UHF radar in Tromsø. The 51 hour continuous run produced 806 debris events. The UHF antenna was parked to the magnetic field aligned direction during the run.

Cp2 campaign 7–29 September at EISCAT UHF radar. From the 545 h measurement, we report here 5151 events, from four antenna parking directions.

Tau0 campaign 11 November at EISCAT Svalbard radar. This 24 hour test measurement produced 650 normal events and 456 “bonus” events (the terms will be explained below).

Manda campaign 17–20 November at EISCAT UHF radar in Tromsø. The 79 h measurement produced 1349 events. The UHF antenna was parked to the magnetic field aligned direction during the run.

The raw data of all the events have been saved to disk. The event parameters are available on the CD accompanying the Final Report of this study.

4.1 Manda campaigns in August 2005 and November 2005

Conceptually, the MANDA experiment is one of the simplest in current use in EISCAT. There is only a single frequency channel. The transmission pulsing is periodic with interpulse period of 1875 μ s. The scheme is intended for the low ionosphere, down to

about 70 km altitude, and provides high spatial resolution. The transmission cycles through a set of 128 different phase codes, each $64 \times 3 \mu\text{s}$ long. The codes are sufficiently different to alleviate the problem of range-aliasing so that one gets unambiguous range to very long ranges. To get coverage throughout LEO, we searched for the return echo in the first seven IPPs after a given transmission. The antenna was parked along the Tromsø magnetic field-aligned direction, azimuth 184.1° and elevation 77.4° . In EISCAT, this pointing geometry is referred to as the CP1 mode. The short IPP of the MANDA transmission results in several blind zones in LEO.

In both MANDA campaigns, target detection was done using FMF with coherent integration of 160 pulses ($T_c = 300$ ms). In DSCAN processing, after each integration, the next 80 pulses were skipped to speed the scanning. For the same reason, only every third range gate, total of 1427, was computed. The velocity interval $\pm 5 \text{ km s}^{-1}$ was monitored. After detection, cleaning, and archiving, the events were analyzed in several ways. The plots shown in Fig. 6 are from analysis done using FMF-based 0.2 s coherent integration.

Both of the MANDA campaigns were scheduled for the time of a meteor shower. Even though the coherence time of meteor echoes is short, and the typical radial velocity much higher than the $\pm 5 \text{ km s}^{-1}$, it turned out that several tens of such echoes were picked up, all below 150 km altitude, in the standard detection scans. In order not to distort SD event count by meteor events, it was necessary to restrict plotting and event counting to altitudes larger than 150 km. We re-scanned off-line the recorded data, with DSCAN better optimized for high-velocity targets with short coherence time. We used the FMF algorithm but integrated coherently only over four pulses. We also used the maximum velocity window allowed by the 2 μs sampling rate. We analyzed the events using non-coherent integration of two pulses. We refer to these events as MANDA-METEOR events; they have been archived separately from the standard space debris events. In the August MANDA-METEOR data we found 2201 events, or 43 events per hour; and in the November data, 3653 events, corresponding to 46 events per hour. Our analysis of the meteor events is good for quick-look purpose, at most. For instance, velocity wrapping should be done more carefully. The extend of velocity values in the data is larger than the about $\pm 40 \text{ km s}^{-1}$ that can be fitted in a single Nyquist zone when using 500 kHz sampling on a 930 MHz radar. In the analysis, we have mapped events with an apparent v_r larger than $+10 \text{ km s}^{-1}$ to $v_r - 80 \text{ km s}^{-1}$. The RCS estimates assume that the target is at the beam center and that the signal is coherent over the pulse duration. A few examples of the meteor data from the November 2005 campaign are in Fig. 7.

4 Measurements

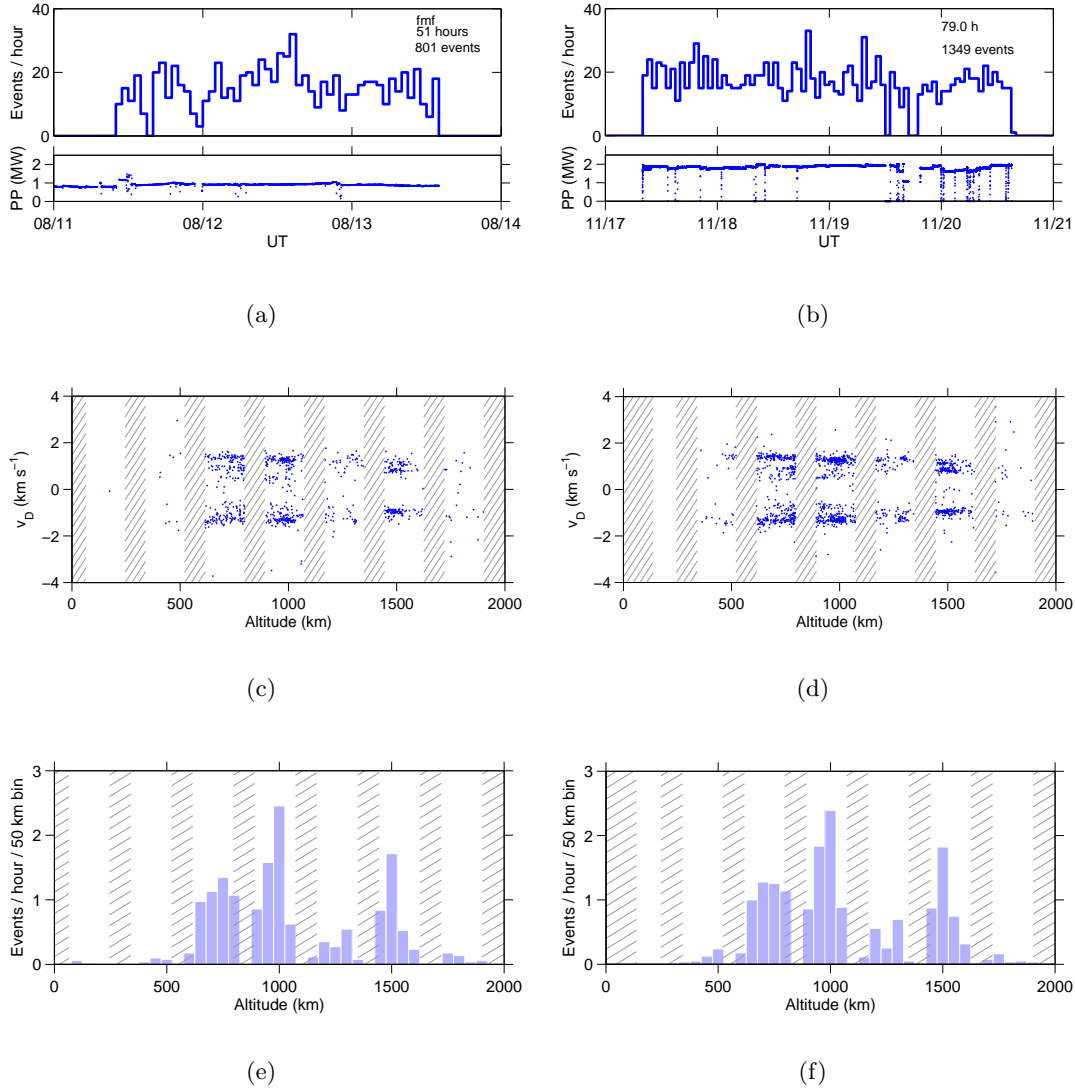
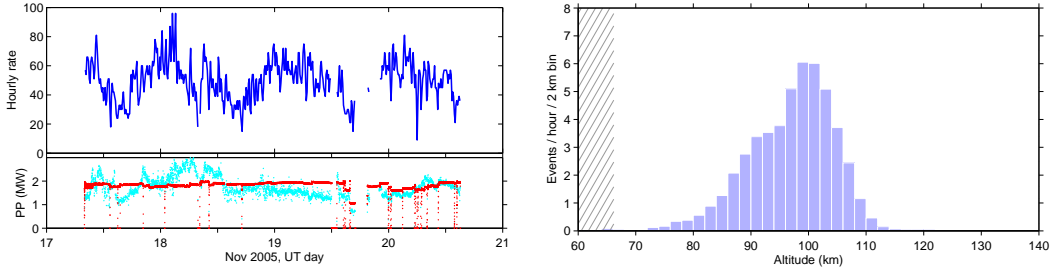


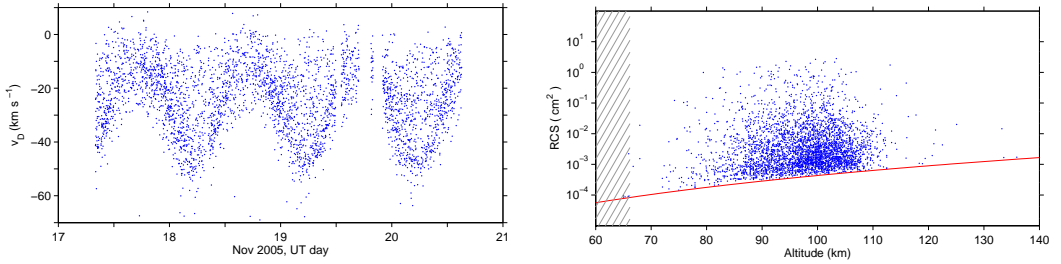
Figure 6: Summary plots of the MANDA campaigns, 11–13 August (Panels a,c,e), and 17–20 November 2005 at Tromsø UHF. The UHF antenna was parked to magnetic field-aligned direction, azimuth 184.9° and elevation 77.4° . The observations shown here exclude altitudes below 150 km, where a large number of meteor events took place. Detection was done with the FMF-algorithm, using 0.3 s coherent integration. Parameter estimation was done with FMF using 0.2 s integration time.

4.1 MANDA campaigns in August 2005 and November 2005



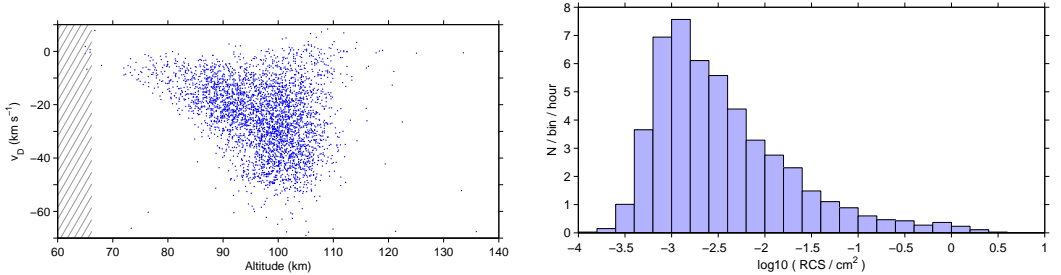
(a) Hourly event rate (one hour moving average), and transmission peak power.

(b) Event rate as function of altitude.



(c) Radial velocity v time.

(d) Radar cross section v altitude.



(e) Radial velocity v altitude.

(f) Event rate v cross section.

Figure 7: Analysis summary plots of 3653 MANDA METEOR events 17-20 November 2005, analyzed with non-coherent integration of two pulses. Panel (a) shows a clear diurnal variation in the number of observed events. In the bottom sub-panel of panel (a), the red points give the peak transmission power as reported by the standard EISCAT ionospheric data analysis, while the cyan points give the power as deduced from the transmission samples recorded by the SD receiver (in the data analysis for effective cross section, panel (d), a constant peak power 1.8 MW was used). Panel (b) gives the altitude distribution of the events. There is a curious-looking bump at around 90 km altitude. Panel (c) shows the Doppler-velocity; there is strong diurnal variation, with the largest magnitudes at about 06 local time, when the radar rams head-on into the sun-orbiting meteoroid cloud. Panel (d) gives an “effective” radar cross section, computed with the same formula, Eq. (15), that we use for the debris events.

4.2 CP2 campaign in September 2005 at Tromsø UHF radar



The EISCAT common mode experiment CP2 has a six-minute, four-position antenna scan. The transmission scheme in the September measurement was the TAU2 pattern, which uses two frequency channels. In most years up to 2005, EISCAT has run enough hours with a CP1-type, fixed-position mode, and that is what the debris software has been tailored for. But 2005 was exceptional, and to be able to collect the agreed amount of data, we decided, (too) late in summer 2005, to cover the CP2. To be able to use as much as possible of the existing software we decided to split the data into position-wise streams. Each pointing direction would be recorded into its own, short data stream when the antenna was stationary. The recording would be stopped while the antenna was changing pointing direction. This would result in four data sets, each corresponding to a complete, standard-format, stand-alone beam-park experiment, readily manageable with the existing SD software.

With hindsight, stopping the recording every so often was a wrong decision, it would have been better to keep the recording running all the time. Due to a programming error, data recording slipped out of synchronization with the antenna motion. We estimate that we lost about 400 events, or 8% of the total of 5150 events in the 23 day long campaign, due to this error.

In the CP2 campaign, we used 56-pulse (312 ms) coherent integration. After every detection scan, 32 IPPs were skipped.

Figure 8 shows that in spite of the blind zones, due to the different elevations in the four parking positions, the experiment manages to sample the debris distribution peaks at around 1000 km and 1500 km altitudes. Figure 8 shows the effective diameter. There is some kind of discontinuity or “layer” at about 6 cm size. The discontinuity is not present in the radar cross section data from which the effective diameter is derived, so we interpret the discontinuity as an artifact of the simplified cross section model, where we ignore the resonance region by artificially joining the Rayleigh and optical regions at about this target size.

It may be noted that there is considerable amount of structure in the velocity scatter plots of Fig. 9.

4.2 CP2 campaign in September 2005 at Tromsø UHF radar

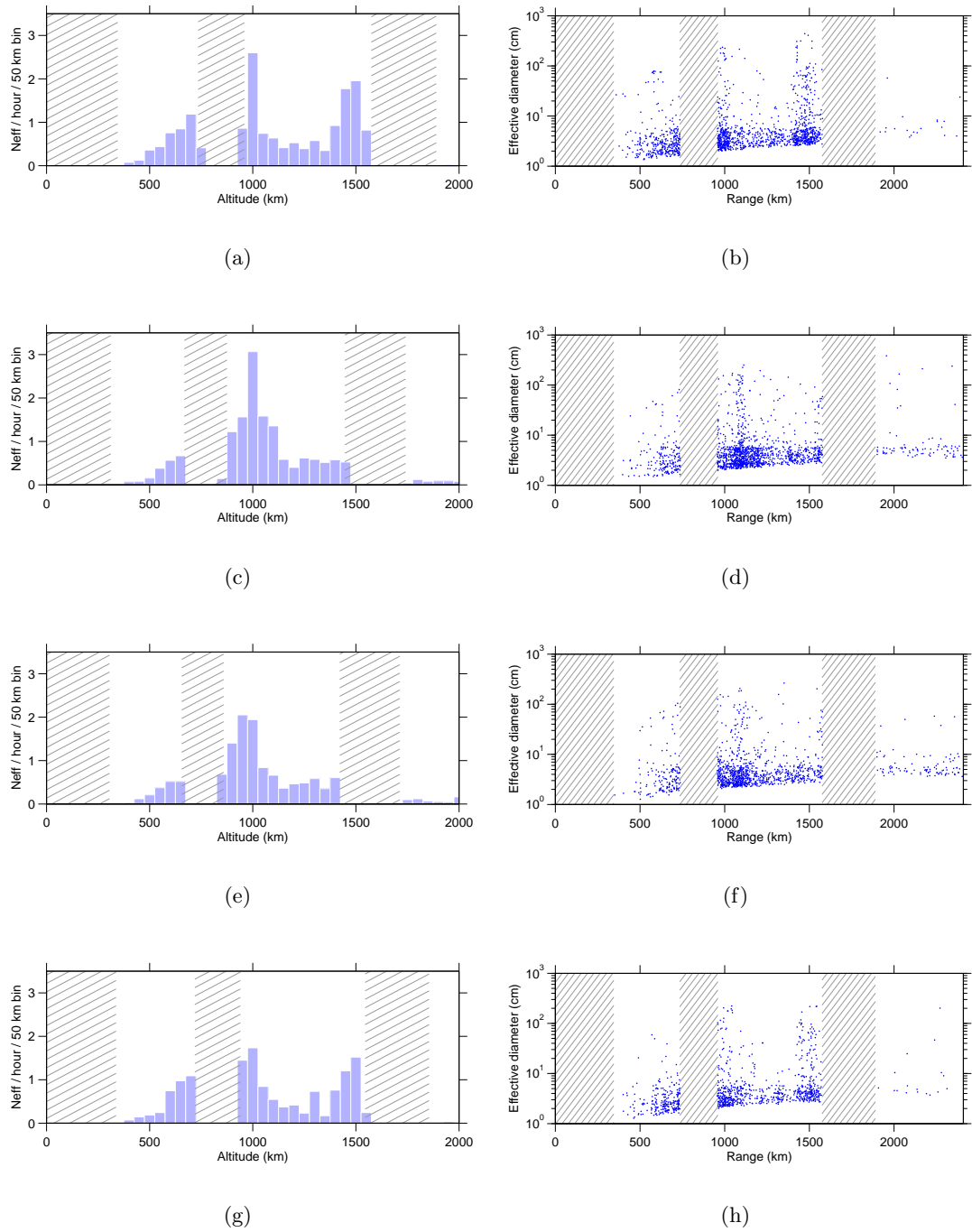


Figure 8: CP2, 7–29 September 2005 at Tromsø UHF. Effective event rate as function of altitude in Panels (a,c,e,g). Effective diameter v range in Panels (b,d,f,h). The antenna pointing directions from top to bottom row are (A 180.0, E 90), (A 165.5.0, E 64.0), (A 133.3, E 61.6) and (A 184.9.0, E 77.4).

4 Measurements

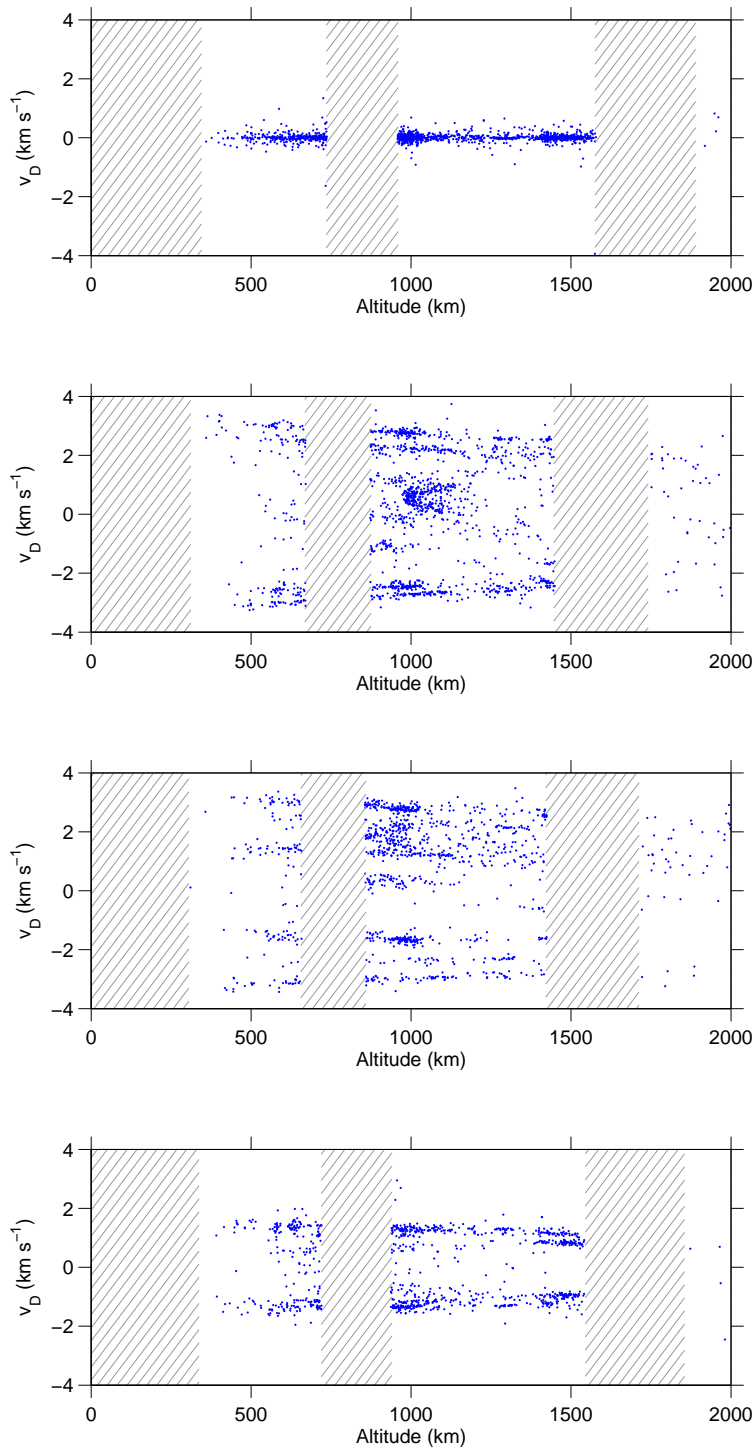


Figure 9: CP2, 7–29 September 2005 at Tromsø UHF. Radial velocity versus altitude in four antenna parking positions. The pointing directions from top to bottom are (A 180.0, E 90), (A 165.5.0, E 64.0), (A 133.3, E 61.6) and (A 184.9.0, E 77.4).



4.3 Test measurement at ESR in November 2005

So far, the 930 MHz UHF radar in Tromsø has been the main instrument for EISCAT's normal work, but the situation seems likely to change in the future, and the emphasis of EISCAT operations is expected to shift over to the 500 MHz Svalbard radar (photo above). Due to the longer wavelength, one would expect the ESR system to be less sensitive for small debris targets than the UHF system. With 0.2 s coherent integration in typical experiments, our standard detection threshold 5.0 corresponds to 2.9 cm effective diameter at 1000 km range at the 42 m ESR system, and 2.5 cm at the Tromsø UHF. The ESR 42 m antenna has half-power beam width about 0.9° (corresponding to 45 dBi gain), which is somewhat more than the 0.6° (gain 48 dBi) beam width of the UHF antenna, and should help to increase the number of detections. The high latitude of the ESR site could also be expected to boost the number of detections, due to the crowding of polar orbits up there. It was clearly worthwhile to check the debris detection sensitivity of the ESR radar with a test measurement.

EISCAT has at the moment two copies of the SD receiver. One unit has been installed in Tromsø, and the other has been kept as a spare in Sodankylä. The spare unit was transported to Svalbard for the test. The SD receiver was configured in the same way as is done in Tromsø.

EISCAT started a scheduled common mode experiment on November 8th, measuring in CP3 mode, using the TAU0 transmission. In CP3 the 32 m antenna pointing direction is cycled through a 14-position meridian scan. In order not to waste the time intervals when the 32 m antenna is re-pointed—EISCAT does not routinely use data from a slewing antenna—those intervals are used to measure with the non-steerable 42 m antenna. In the CP3 mode, the transmission is switched between the antennas every 64 seconds, and only the recording system associated with the active receiver chain is used at any given time. Because the SD receiver was connected to the 42 m antenna, we expected to get useful data only for 64 seconds at a time, interleaved with 64 seconds of noise, but we nevertheless kept the debris recording running continuously.

To make use of the high (up to 25%) allowed duty cycle of the ESR transmitter, the TAU0 transmission uses two $960 \mu\text{s}$ phase-coded pulses in a $9990 \mu\text{s}$ IPP, on two

4 Measurements

frequencies. The pulses are sent closely after each other, with a $60 \mu\text{s}$ gap in between; the $60 \mu\text{s}$ is also the length of a single bit in the 16-bit code. A problem became evident soon after we had started the recording. We had set DROS to produce one hour long data streams; this works nicely in Tromsø. But it now turned out that when DROS tried to re-launch the recording program in the measurement computer for a new stream, the recorder refused to start, and it was necessary to reboot the measurement computer to get the recording started. We wasted considerable number of measuring hours before believing that we had a systematic problem which we could not remedy. To save the campaign, we gave up having the data in hourly directories and recorded the data in much larger chunks. We have not had the opportunity to inspect what actually went wrong with the SD system at ESR. Even so, the recording problem serves as a reminder that for future work, the SD hardware necessarily must be updated and brought under EISCAT control.

Due to these difficulties, we managed to make only a cursory check of the data during the stay on Svalbard, and had to analyze the data off-line in Sodankylä. We ran the standard DSCAN-CLEANSkans-DARC-ANALYSIS chain on all the raw data, irrespective of whether the relevant transmission was supposed to be active (transmission on the 42 m antenna) or inactive (transmission on the 32 m antenna). The result was a twofold surprise.

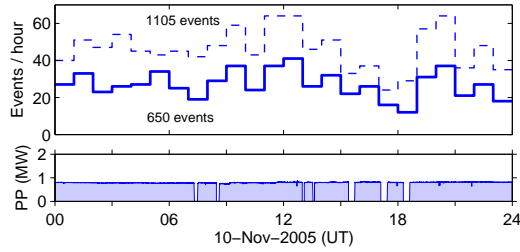
High event rate when the transmission was on the 42 m antenna. When the transmission was on the 42 m antenna, we got more events per hour than we normally observe at the Tromsø UHF radar. Figure 10, panel (a), shows the actual event count per hour, that is, there is no correction for the recording duty cycle. Only those events have been counted that occurred at the times when the transmission was known to be on the 42 m antenna. Obviously, the effective, duty cycle corrected event rate would have been twice as high, about 40 events per hour. That is about 50% higher than we have ever measured at the Tromsø UHF.

High event rate even when the transmission was on the 32 m antenna. Panel (b) of Fig. 10 shows the uncorrected event count for the time intervals when the transmission was known to be on the “wrong” antenna, the 32 m antenna which should have had no connection to the SD receiver. The event count is smaller than on the “correct” antenna, but by no means insignificant. The other panels of Fig. 10 and Fig. 11 show no drastic difference in the parameters of the events between the two data sets, either. We refer to these unexpected events as “bonus” events.

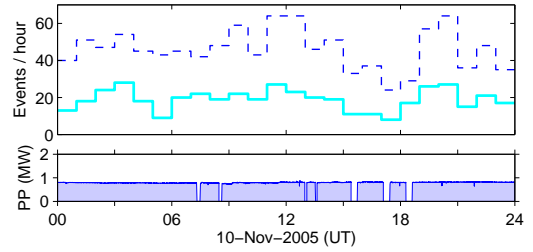
We do not know for certain what caused the bonus events, but we suspect that the switching of the transmission from the 42 m antenna to the 32 m antenna might not have been perfect. The switching is implemented by changing, in the microsecond time scale, the relative phasing of the two RF inputs of a four-port switchless combiner that collects the power from the two halves of the transmitter, and should forward it only to one of the antennas, see Fig. 4. The switch might, in effect, be leaking, causing some residual amount of the transmission power to go to the 42 m antenna.

In conclusion, it is clear that the ESR system is suitable for space debris measurements. As was clear at the outset, the detection sensitivity is slightly lower than we get at the Tromsø UHF, but the good event statistics, the often available long measurements, and the excellent system stability, more than compensate for the handicap caused by the longer wavelength. We are looking forward for opportunities to resume EISCAT space debris measurements, full-scale, and now using the most modern of the EISCAT systems.

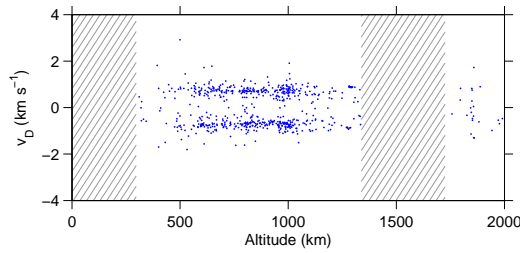
4.3 Test measurement at ESR in November 2005



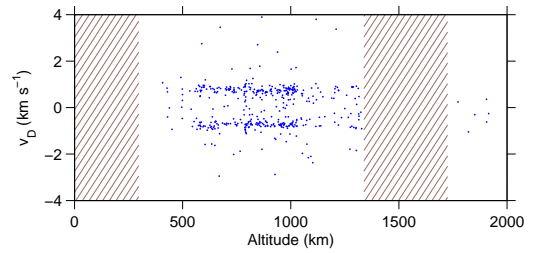
(a) Hourly event count and transmission peak power for events recorded when the transmission was through the 42 m antenna.



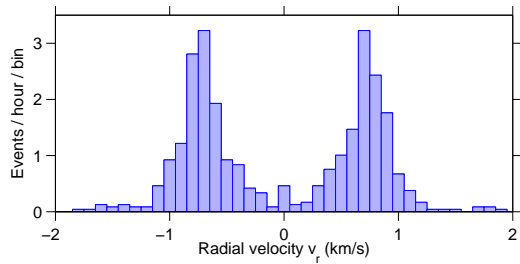
(b) Hourly event count in the data recorded by the SD receiver (hooked to the 42 m antenna) when transmission was through the other, 32 m, antenna.



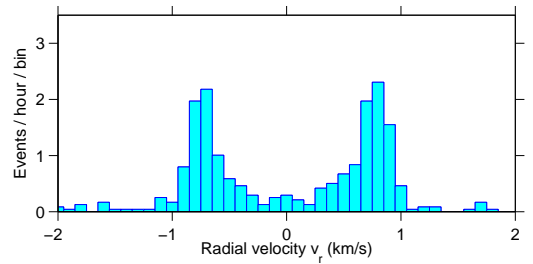
(c) Radial velocity and altitude in the standard events.



(d) Radial velocity and altitude in the bonus events.



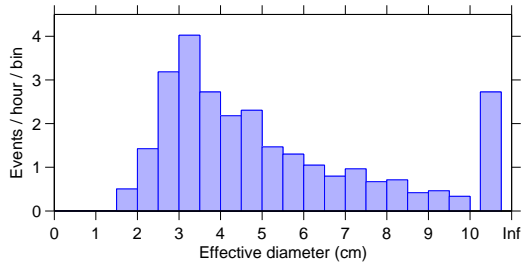
(e) Mean event rate as function of radial velocity in the standard events.



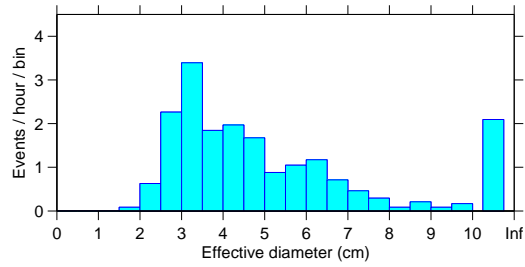
(f) Mean event rate as function of radial velocity in the bonus events.

Figure 10: TAU0, 10 November 2005 at EISCAT Svalbard radar.

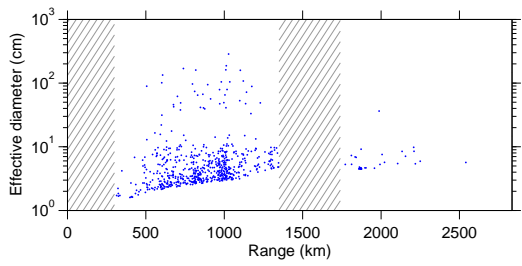
4 Measurements



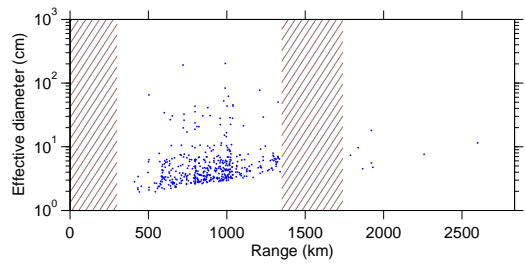
(a) Mean event rate as function of target diameter for the standard events.



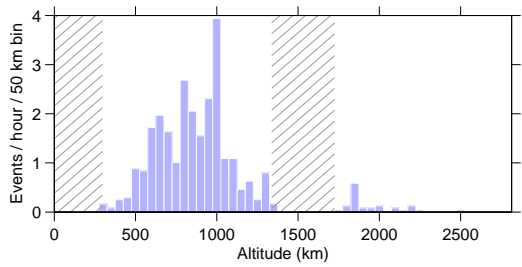
(b) Mean event rate as function of target diameter for the bonus events.



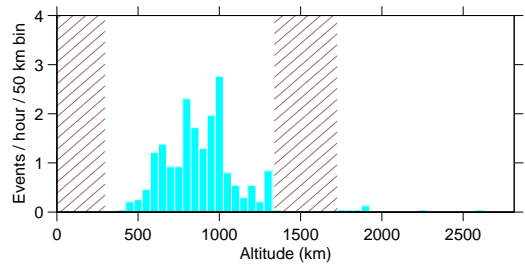
(c) Effective diameter and range of the standard events.



(d) Effective diameter and range of the bonus events.



(e) Event rate as a function of altitude for the standard events.



(f) Event rate as a function of altitude for the bonus events.

Figure 11: TAU0, 10 November 2005 at EISCAT Svalbard radar.

References

- [1] M. Baron, The EISCAT facility, *J. atmos. terr. Phys.* **46** (1984) 469.
- [2] M. Baron, EISCAT progress 1983–1985, *J. atmos. terr. Phys.* **48** (1986) 767.
- [3] ESA Directorate of Technical and Operational Support ESOC Ground Segment Engineering Department Mission Analysis Section, *Study specification, measurements of small-size debris with backscatter of radio waves* (Darmstadt, Germany, 1999).
- [4] ESA Directorate of Technical and Operational Support ESOC Ground Segment Engineering Department Mission Analysis Section, *Study specification, real-time space debris detection with EISCAT radar facilities* (Darmstadt, Germany, 2002).
- [5] ESA Directorate of Technical and Operational Support ESOC Ground Segment Engineering Department Mission Analysis Section, *Study specification, small-size space debris data collection with EISCAT radar facilities* (Darmstadt, Germany, 2004).
- [6] J. Markkanen, M. Lehtinen, A. Huuskonen and A. Väänänen, Measurements of Small-Size Debris with Backscatter of Radio Waves, (Final Report, ESOC Contract No. 13945/99/D/CD, 2002).
- [7] J. Markkanen and M. Postila, Real-time Small-Size Debris Detection with EISCAT Radar Facilities, (Final Report, ESOC Contract No. 16646/02/D/HK(SC), 2005).
- [8] J. Markkanen, M. Lehtinen and M. Landgraf, Real-time space debris monitoring with EISCAT, *Advances in Space Research***35**(2002) 1197-1209.
- [9] J. Markkanen, M. Postila and A. van Eyken, Small-Size Space Debris Data Collection with EISCAT Radar Facilities, (Final Report, ESOC Contract No. 18575/04/D/HK(SC), 2006).
- [10] G. Wannberg, I. Wolf, L.-G. Vanhainen, K. Koskenniemi, J. Röttger, M. Postila, J. Markkanen, R. Jacobsen, A. Stenberg, R. Larssen, S. Eliassen, S. Heck and A. Huuskonen, The EISCAT Svalbard radar: A case study in modern incoherent scatter radar system design, *Radio sci.* **32** (1997) 2283.